Material and Geometry Factors in Joint Design of Electronic Equipment to Minimize Electromagnetic Interference

BEHZAD D. MOTTAHED,[1] SOURAN MANOOCHEHRI[2]

[1] Bell Laboratories, Lucent Technologies, Whippany, New Jersey

[2] Mechanical Engineering Department, Design and Manufacturing Institute Stevens Institute of Technology, Hoboken, New Jersey

Received 20 April 1996; accepted 11 December 1996

ABSTRACT: Reducing electromagnetic interference in electronic equipment is of great importance. This is normally accomplished by increasing the shielding effectiveness of the enclosure. In this study, shielding effectiveness is examined against enclosure material, joint geometry, and operating frequency. An experimental apparatus is designed and manufactured to aid in finding the suitable joint configurations and materials with high shielding effectiveness. Three groups of material, namely, metallic, filled polymers, and metalized filled polymers, are investigated. In addition to the choices of material, effect of joint configurations on shielding behavior are examined. Based on the experimental results, empirical relations are developed that relate shielding effectiveness to effective length, shape factor, and aperture dimensions of the joint structure. Finally, the best material and joint geometry among the investigated cases are presented. © 1997 John Wiley & Sons, Inc. J Appl Polym Sci **64:** 1667–1679, 1997

Key words: aperture; joint design; shielding effectiveness; EMI/EMC; electronic equipment

INTRODUCTION

In recent years, many investigations have been conducted related to the electrical/mechanical design of electronic enclosure in low and high frequency domain. In the past, electronic enclosures (such as cabinets and board level packs) were built out of metals. However, with advances in the field of polymers, engineers are shifting more towards the application of these materials in the design and manufacture of electronic enclosures. An enclosure assembly consists of many electrical and mechanical components. Among them, those related to the enclosure body, mating joints, printed wiring board, and gasketing are of importance for reduction of electromagnetic interference.

The two-half enclosure made of metal or polymeric materials consists of various features. The enclosure body needs to be designed to provide holes for cooling, input-output ports for electrical connections, hinges, joints, etc. The enclosure wall needs to satisfy the structural requirements due to applied loads such as static, impact, shock, and other requirements.

Materials used in the design of high frequency electronic enclosure (either consumer products or otherwise), in general, need to exhibit the following characteristics:

1) sufficient electromagnetic interference (EMI) shielding effectiveness;
2) mechanical strength to withstand various loading;

Correspondence to: B. D. Mottahed.

Contract grant sponsors: Bell Laboratories at Lucent Technologies and Design and Manufacturing Institute at Stevens Institute of Technology.

3) matched thermal expansion with other system components;
4) adequate creep and stress relaxation properties;
5) resistance to corrosion;
6) dimensional stability;
7) surface quality.

In this study, efforts are directed towards satisfying shielding requirements. It is assumed that other above-mentioned criteria need to be satisfied simultaneously. Selection of material used on the design, openings on the enclosure, frequency of operation, and the configuration of the joints are some of the main parameters affecting the electromagnetic shielding design of electronic equipment.

Undetected interference causes the malfunctioning of electronic devices. This leakage plays a major role in reduction of the shielding between the compartments of small and large enclosures. Not only the joint geometry, but also the material making the jointed surfaces, has a strong effect on the shielding effectiveness.

The use of polymeric materials in design of electronic enclosure has many advantages and some disadvantages.[1] Since most polymeric materials are inherently nonconductive, impregnentation by metal particles such as stainless steel, nickel-coated graphite is one technique to provide electrical conductivity. Another technique is to metalize the surface of the polymer by a combination of copper and nickel to enhance shielding properties. There are numerous articles,[2–14] dating from early 1970s, that look at these properties; however, none have investigated the combination of material selection and the joint geometry together.

A mathematical tool was presented by Railkar et al.[15] to calculate the electromagnetic fields in the shielded enclosure using Maxwell equations. Some investigators[16] have reported the experimental study of narrow slot with cavity-backed enclosures; however, only one joint configuration was reported. Gedney and Mittra[17] and Auckland and Harrington[18] examined the joint geometry and modeled the effect of some joints on EMI shielding effectiveness. Honig[19] experimentally investigated the effect of predetermined flaws, such as cracks, lack of fusion, and porosity on EMI shielding.

Mohr[20] presented an evaluation technique for EMI seams using gasketed and non-gasketed joints. Merewether[21] studied the knife-edged joint, utilizing the voltage dividing technique to assess the improved shielding for frequencies between 10 MHz to 1 GHz. For large-scale construction, Miyake et al.[22] evaluated various seams, joints with various fastener spacing, fastener types, and materials.

A low frequency approximation of the generalized network formulation based on the assumption that the slot is very narrow (width $W \ll$ wavelength λ) was presented in Senior and Volakis.[23] Impedance boundary condition (IBC) is used to compute the scattered fields in a narrow aperture. For $W < 0.15\lambda$, a good agreement was noted for both transverse magnetic (TM) and transverse electric (TM) polarization.[24] Utilizing finite element methods, Jeng and Tzeng[25] analyzed the two-dimensional TM wave scattering from a cavity-backed slit in a ground plane.

Murthy[26] examined the overall losses in thermoplastic materials, having overlapped joints. Additionally, packaging design to reduce the EMI propagation was studied by Pettit[27] and Steinfeld.[28]

Auckland and Harrington[29] developed a solution for computing the transmission characteristics of a slit in a conducting plate of finite thickness placed between two media. The equivalent principle was used to solve this TE case. Another approach to solve the apertures with depth and losses was described by Warne and Chen.[30] A problem of narrow slot aperture in thick conducting plane was investigated by these authors for the case of high conductivity but not infinity. In this study, the transmission line theory was used to determine the antenna modes along the slot. Addition of gasket was also considered. The slot voltage was assumed to be nearly constant over the local region. The local transmission theory allowed the effect of losses due to the gasket and the walls to be modeled. The analysis was performed for a rectangular slot with and without gaskets.

One other technique to solve the shielding effectiveness of an enclosure is circuit approach. Bridges[31] developed equations describing the penetrating fields. This technique not only includes the details of the geometry but also includes the effects of the properties of the shielding material, effect of resistive seams in the enclosure walls, and a nonempirical consideration of mesh enclosure. Vitek[32] provided a method of predicting the shielding effectiveness (SE) of rectangular apertures. The author made use of special transverse

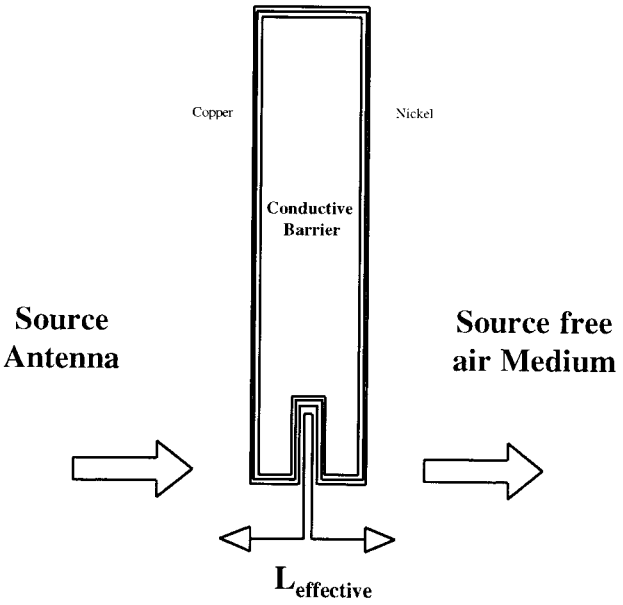

Figure 1 Anatomy of a joint.

electromagnetic (TEM) cell to simulate far-field behavior.

Utilizing metal (aluminum), Mottahed and Manoochehri[33] investigated the effect of gaps between various joints to determine the level of degradation of SE and predicted the relative shielding values. Increasing the slope of the angle of a joint geometry causes the shielding effectiveness to increase, approaching the SE of a barrier of the same material with no joint. It was concluded that the addition of bends in the joint geometry increases the shielding effectiveness. Furthermore, the introduction of a gap for both simple and complex joint configurations, caused by tolerances on the parts or clearances between parts, furnishes almost identical shielding reductions, which was asymptotically depleting.

Theoretically, EMI shielding of conductive barrier exposed to radiation can be described as follows.

There are three regions in the system (shown in Fig. 1) as follows:

a) source antenna (region of the EM generation);
b) the conductive medium;
c) source-free medium (the region where the EM field need to be protected).

In the region (a), the EM field can be represented by Maxwell equations having vector and scalar potentials. In the region (b), there could be losses due to existence of joints, seams, and venting holes. It is in this region that most of the protection against penetration of EM occurs. In region (b), the electric field intensity is related to the current in the medium by the conductivity of the solid medium or the capacitive coupling of the medium in the case of partially metalized medium, (i.e., metal filled polymers).

In region (a), electromagnetic field can be defined by the following potential functions:

$$A(\bar{E}, t) = \frac{\mu}{4\pi} \frac{\bar{J}\left(r, t - \frac{R}{v}\right)}{R} dv' \qquad (1)$$

$$V(\bar{r}, t) = \frac{1}{4\pi\varepsilon} \frac{\rho\left(r, t - \frac{R}{v}\right)}{R} dv' \qquad (2)$$

where J and ρ are the current and charge densities, and μ and ε are permeability and dielectric constants of the medium, respectively.

The simplified differential equations pertaining to the region (a) are

$$\nabla^2 \bar{A} = -\mu \bar{J} \qquad (3)$$

$$\nabla^2 V = -\frac{\rho}{\varepsilon} \qquad (4)$$

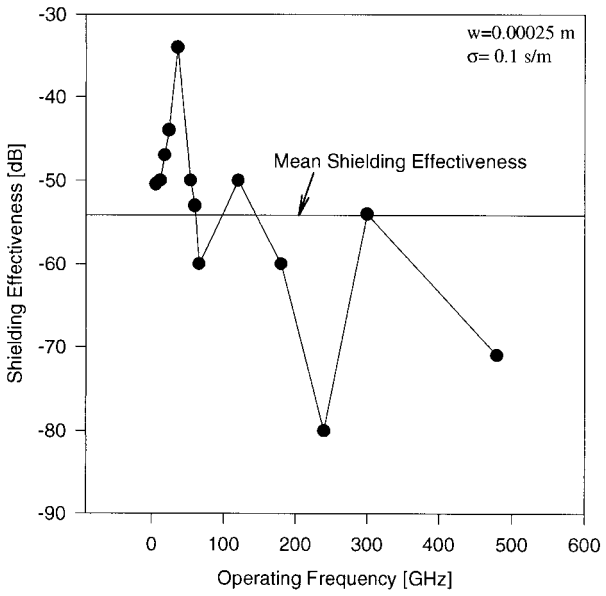

Figure 2 Driven analytical results for an overlap joint.[17]

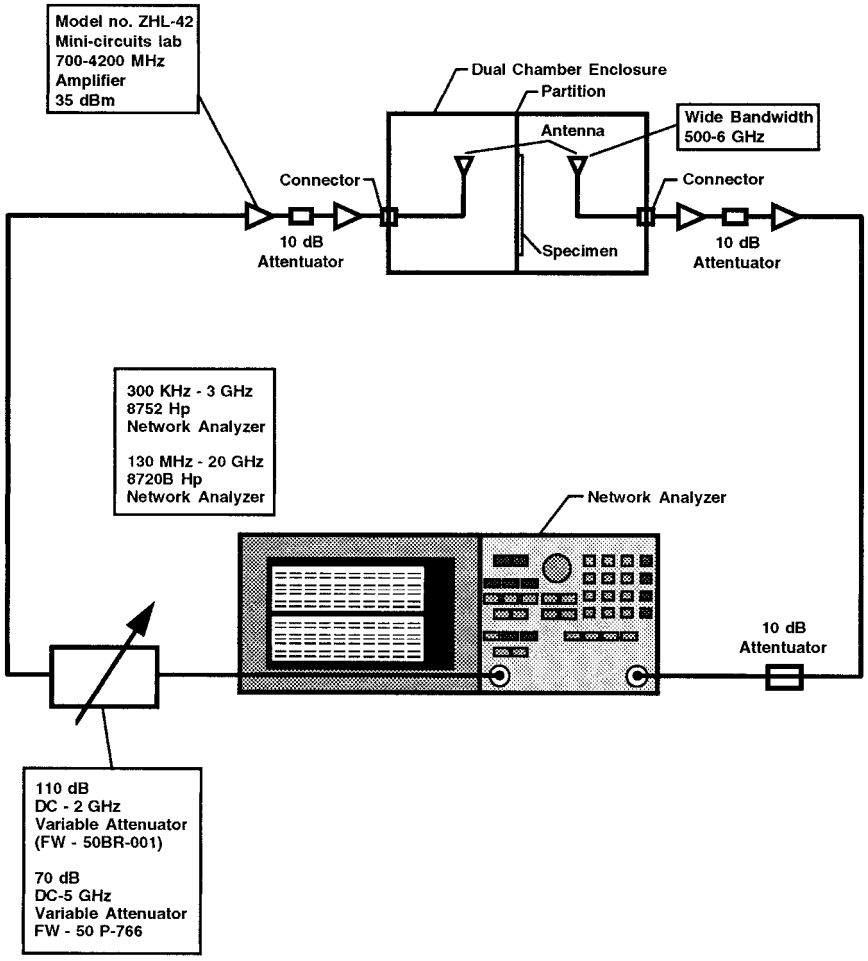

Figure 3 Schematic drawing of the experimental setup.

E and H, (electric and magnetic) fields can be derived from the above potential equations as:

$$\bar{E} = -\nabla V - j\omega\bar{A} \tag{5}$$

$$\bar{H} = \frac{1}{j\omega\varepsilon}\nabla \times \bar{E} \tag{6}$$

For the conductor region, the EM field is obtained from

$$\nabla^2\bar{E} - (\omega^2\mu\varepsilon + i\omega\mu\sigma)\bar{E} = 0 \tag{7}$$

$$\nabla^2\bar{H} - (\omega^2\mu\varepsilon + i\omega\mu\sigma)\bar{H} = 0 \tag{8}$$

Since the conductivity σ is approximately zero in region (c), the above equations can be simplified to

$$\nabla^2\bar{E} - \omega^2\mu\varepsilon\bar{E} = 0 \tag{9}$$

$$\nabla^2\bar{H} - \omega^2\mu\varepsilon\bar{H} = 0 \tag{10}$$

These equations have been solved in literature for some simplified configurations and assumptions. For example, Gedney and Mittra[17] have presented the solution to the problem of electromagnetic transmission through inhomogeneously filled slot in a thick conducting plane. The authors studied the effect of electromagnetic penetration on a butt and overlap joint of electrically conductive plane with various angles of incidence. They utilized finite element method/method of moment algorithm to numerically solve the electromagnetic transmission through a joint. The results of their work are presented with various graphs relating the P_t/P_{inc} to the $2w/\lambda$, where P_t is defined as the transmitted power, while P_{inc} is the incident power on the joint. Figure 2 illustrates a data reduction done by the current authors from the above work for an overlap joint. The available data for calculation of shielding effectiveness is for frequencies above 6 GHz, which represents a different frequency range than that are often used

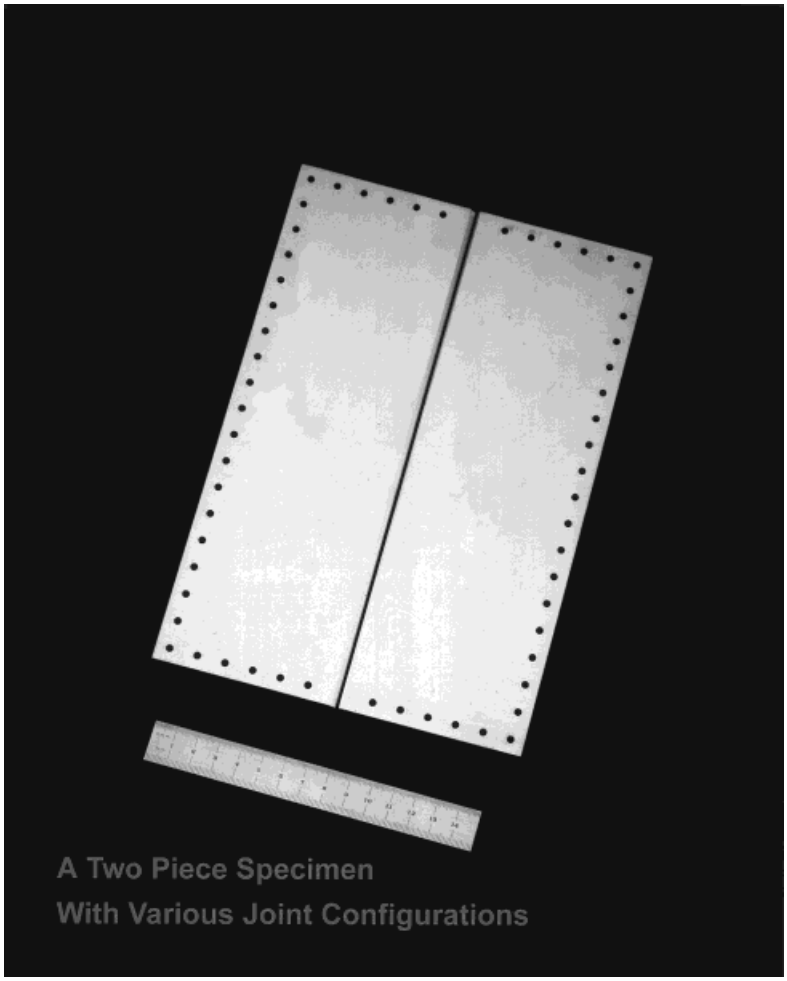

Figure 4 A sample of interlocking joints.

in design. The shielding effectiveness at 6 GHz, for TE wave, having w (width of the material) of 0.0258 cm, and moderate material conductivity is calculated to be −50 dB. The mean shielding effectiveness of this joint, for the range of frequency shown in the figure, is −54 dB.

From the review of the literature, it can be concluded that a general solution for these equations for different joint and material conditions are not trivial. In addition, experimental results for verifications of these solutions are scarce. Thus, the main objective of the present study is to generate experimental results that can be used to validate the theoretical modeling of some of the joints based on the above mentioned equations.

To accomplish this task, a dual-chamber experimental apparatus is constructed to measure the relative SE of the specimens. These measurements are made within a 0.7–4.2 GHz frequency range. In the Experimental Analysis Section, the experimental setup is described, followed by description of joint anatomy in the Joint Anatomy Section. Empirical evaluation of various joints and a design methodology are reported in the Results and Discussion Section.

EXPERIMENTAL ANALYSIS

A complete schematic of the circuit and dual-chamber apparatus used to measure the SE values (see Wilson and Ma[34] for similar testing technique) is shown in Figure 3. A signal generated by port 1 of the network analyzer is amplified by two series-connected amplifiers. Double-shielded coaxial cables conduct the amplified signal to one of the enclosure cavities. The signal is then conducted to the emitting dipole-conical antenna, having a wide bandwidth from 500 MHz to 6 GHz and is picked up by an identical antenna located

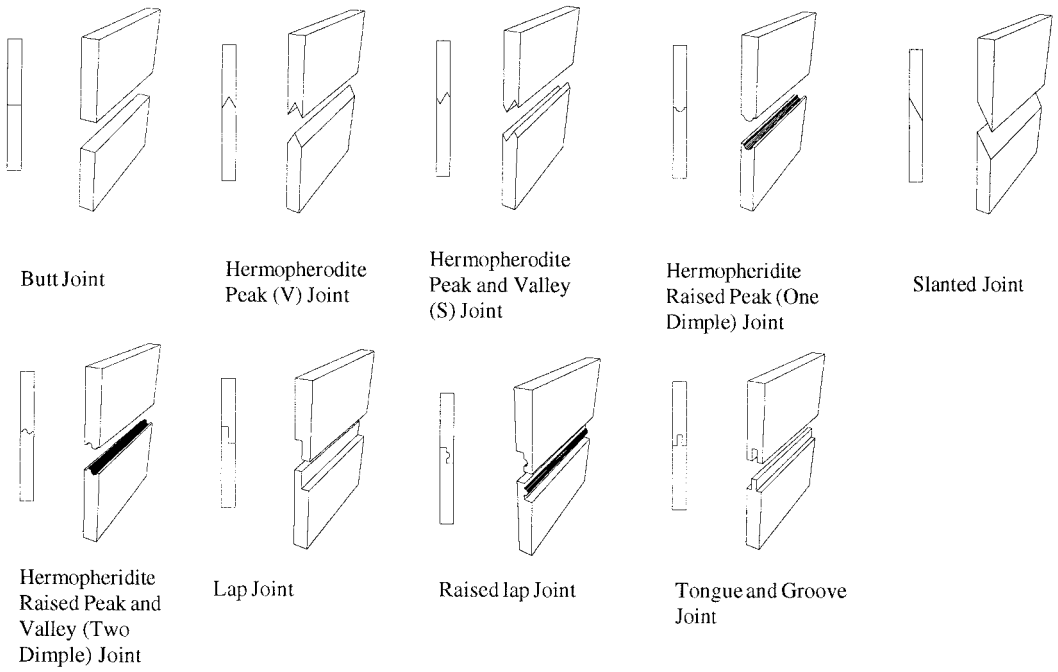

Figure 5 Various joint configurations.

in the second chamber. The antenna's signal is amplified by two additional amplifier stages prior to returning to port 2 of the network analyzer.

The apparatus consists of two half-enclosures made of aluminum having mounting holes and plate for attachment of specimens. The cavities are covered on all sides with absorbing material to reduce higher order standing waves interfering with the experimentation. Even for TEM and other measurement techniques, some standing waves are observed.[35,36] The specimens are attached to the mounting plate (made of aluminum) by 4–40 size screws, designed to be 12.7 mm apart for best protection against EMI penetration; however, experiments indicate that fasteners need not be less than 25.4 mm apart to provide the same results. Figure 4 shows sample of an interlocking joints. The specimens are mounted in front of the enclosures prior to the experimentation. On the periphery of the front of the enclosures, two rows of Beryllium–Copper fingerstock are installed to provide the highest shielding through the enclosures. Furthermore, around the mounting plate where the specimens are attached, similar fingerstocks are used to prevent any leakage through the side openings.

JOINT ANATOMY

A detailed anatomical drawings of a joint is shown in Figure 1. In this figure, regions of emitted electromagnetic field, inner joint, and the outer joint are shown. These joints are machined either from plain aluminum or polymer-based specimens molded from polycarbonate with filled metals. The fillers are either stainless steel or nickel-coated graphite impregnated in the polymer. In some cases, polycarbonate filled with nickel-coated graphite is further metalized using electroless plating. The surfaces of the specimens are plated with copper and nickel, mainly for protection against far and near-field effects, respectively. The thickness of copper and nickel applied to both sides of the specimens are 1.5 and 0.4 μm, respectively. The tolerances specified on the finished part are ± 0.012 mm. The two-piece specimens shown in the figure are 241.3 by 88.9 by 3.175 mm each. Many pairs of mating joint surfaces are designed to interlock with minimum clearance. Figure 5 gives the schematics of all joint configurations studied in this work. Figure 6 shows a photography of one of the specimens prepared for this study.

As shown in Figure 5, butt joint consists of two touching flat surfaces with 90 degree inclination angle from the vertical direction. If the inclination angle is less than 90 degree, the joint is categorized as the hermaphrodite slanted joint. The third joint configuration under study is a hermaphrodite raised peak (dimple) joint that consists of two concentric cylindrical bodies. The V

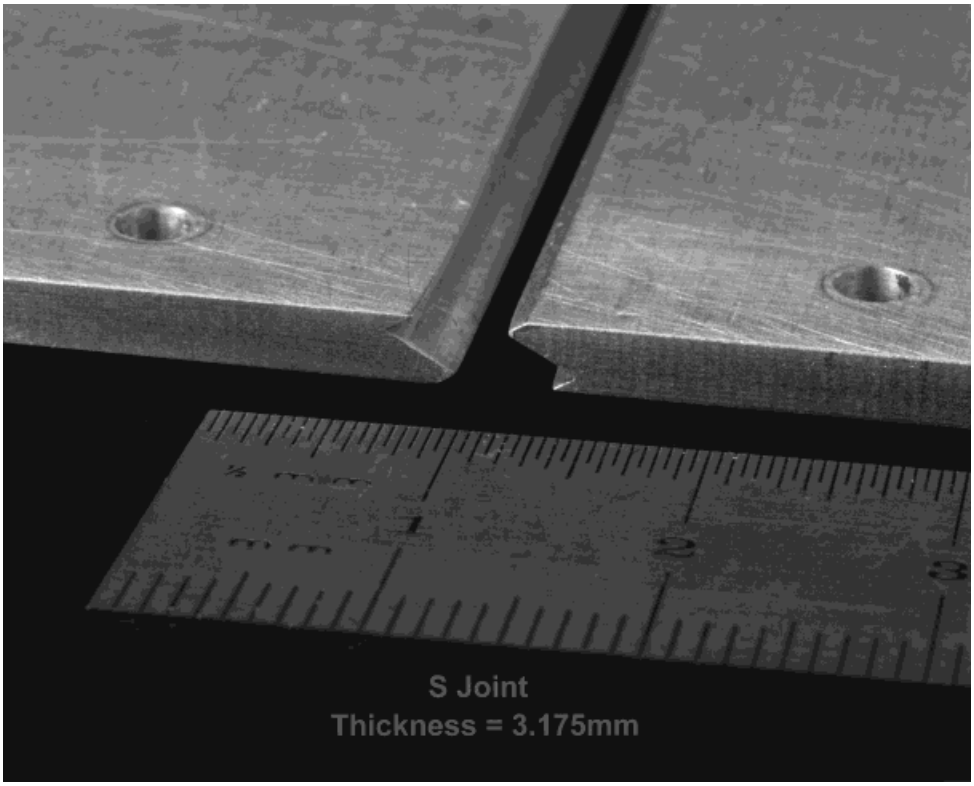

Figure 6 Sample specimen: hermaphrodite peak and valley *S* joint.

joint is defined by a double slanted surfaces at the interface. The hermaphrodite peak and valley (*S*) joint provides flat crisscrossing joint surfaces. The double-dimple joint combines two dimple joints in reverse directions in series. The remaining three are lap, raised lap, and tongue and groove joints. The raised lap joint is in the family of lap joints, while the tongue and groove, one-dimple, and *V* joints essentially are in a different family. Likewise, two-dimple and *S* joints belong to another family of joints. The joints listed in Figure 5 start with simple configurations and progressively increase in their complexity. This added complexity relates to increased cost and manufacturing difficulties; however, it may result in a better mating and mechanical strength that require less fasteners to enhance joint rigidity. The clearance between the two mating joint surfaces is designed to be less than ± 0.025 mm.

A large solid 241.3 by 177.8 by 3.175 mm plate is also fabricated as a reference for maximum shielding measurements obtainable with this given test apparatus. This gauge is the baseline for the best shielding possible with the chosen material, namely, aluminum.

A pair of mating plates characterized by the material and joint geometry is mounted on the evaluation plate and secured by many screws. Extra care is taken to assure good mating of the joining surfaces (such as having a clean mating surfaces). The screws are used to mount and torque down the specimens preset for 5 lb/in (3.688 N/m) of torque. The plate is then mounted on the opening side of the chamber, and the two chambers are fastened by screws securely every 38.1 mm apart. The gaps introduced between the mating joints are accomplished by premeasured plastic sheet gauges, which are accurate to ± 0.0084 mm. The signal generated by HP network analyzer is amplified, transmitted, and received, then reamplified and returned to the HP network analyzer.

To measure shielding effectiveness directly, two measurements have to be performed to minimize the effect of all variables except materials and joint configurations. These measurements are made as follows: a) measurement of the S_{21} of the signal transduced with the aperture fully opened and without the presence of the joint plates; and b) measurement of the S_{21} of the signal transduced with the specimen mounted in the aperture spacing inserted. Shielding effectiveness (SE) is

thus defined in the following as the difference between S_{21} transmitted between two antennae in test fixture, with and without the specimens in place.

$$\mathrm{SE} = (S_{21(\mathrm{AFTER})} - S_{21(\mathrm{BEFORE})}) \qquad (11)$$

where S_{21} is defined in dB.

Furthermore, SE can be defined for magnetic or electric field as a transfer function for magnetic or electric fields as follows:[37]

$$\mathrm{SE} = 20\,\mathrm{Log}\left[\frac{\text{magnetic field inside cavity}}{\text{mag. field in the absence of shield}}\right] = 20\,\mathrm{Log}\left[\frac{\text{electric field inside cavity}}{\text{elec. field in the absence of shield}}\right] \qquad (12)$$

SE can also be defined as follows:[36]

$$\mathrm{SE} = 10\,\mathrm{Log}\left[\frac{P_{\mathrm{in}}}{P_{\mathrm{after}}}\right] \qquad (13)$$

where P_{in} and P_{after} are powers measured with fully open aperture and with specimen inserted, respectively.

To make sure all the measurements are made with respect to one reference point, on the onset of the experimentation, the half-enclosures are attached to each other without the dividing plate, and the adjustable attenuator is set to 50 dB to prevent possible overloading of the amplifiers. The calibration is made with respect to this condition, and the reference level on the network analyzer is set to zero at this time. The specimen is attached to the enclosure and to the interface between the testing plate and the two cavities. The final result for each test is the measured value plus 50 dB. If the values are less than 110 dB (dynamic range of the system), 50 dB of the attenuation can be removed, and the relative reading of the network analyzer will be observed.

After applying the power, the relative SE is shown on the network analyzer with respect to the no specimen condition, already in dB.

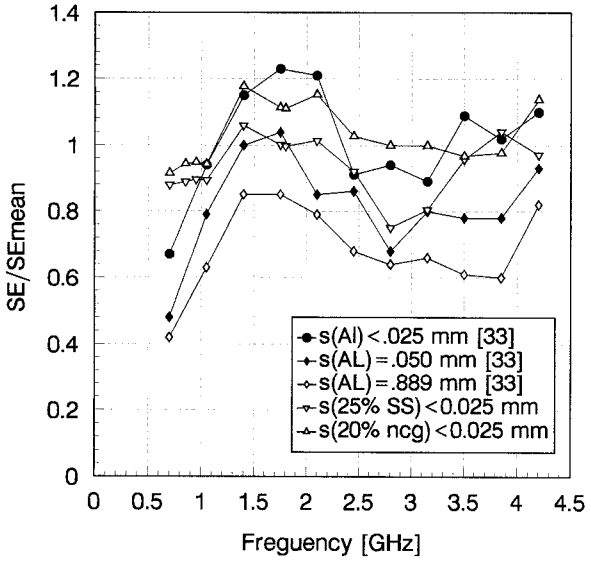

Figure 7 Shielding effectiveness of butt joint with various materials.

RESULTS AND DISCUSSIONS

Figure 7 illustrates the effect of material selection on the shielding effectiveness of the simple butt joint (HBJ). Shielding effectiveness dependency on the material selection of the jointed parts are well presented in the figure, where the abscissa represents the range of frequency used in the experimental evaluation, and the ordinate shows the ratio of SE of each condition versus the mean value of the best condition (S = 0.0254 mm), [β = $\mathrm{SE}/\mathrm{SE}_{\mathrm{mean}}$]. It can be seen that the shielding effectiveness of the aluminum is mainly higher than other materials at frequencies above 1 GHz. Below 1 GHz, the relative shielding tends to be nearly constant for polycarbonate filled with nickel-coated graphite and stainless steel. At these frequencies, β demonstrates to be higher for a butt joint made of aluminum.

Additionally, the effect of presence of gap between the mating joints are also shown.[33] It can be concluded that even though the SE of aluminum is better than the polymeric-based joints, introduction of gap diminishes this advantage to being negligible if the gap is larger than s = 0.40 mm. With larger gaps, the SE suffers substantially unless the operational frequency of the device is around 1.2–2 GHz. It can also be concluded that the differences in the peak to peak shielding values (maximum to minimum values of shielding) is less pronounced in the polymer-based shields than the metals (aluminum). This can be basi-

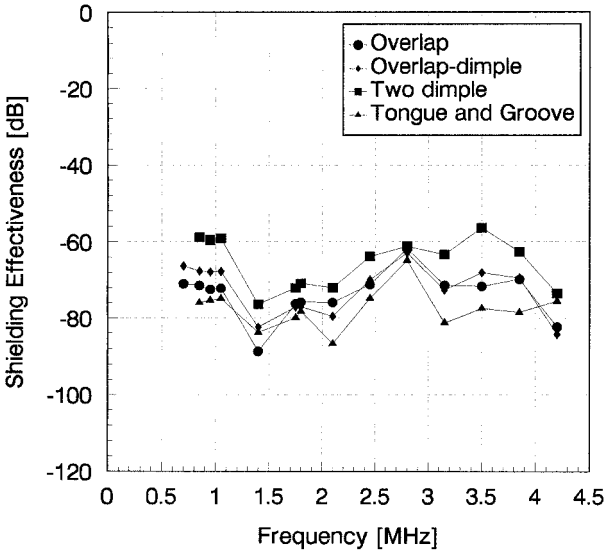

Figure 8 Shielding effectiveness of 20%-filled nickel-coated graphite in polycarbonate having various joint configurations.

cally due to higher absorption characteristics of polymeric-based shields than aluminum. This is an advantage for polymeric materials over metal-based materials, since it covers a larger range of frequencies than aluminum, making it more useful in the full range of frequency of operations, at least for a simple butt joint.

Figure 8 shows a family of curves relating the shielding effectiveness to the frequency of operation. In this figure, four different joints are investigated having various complexities and effective lengths. The overlap joint compares well with the overlap-dimple joint. In terms of assembly, the latter one provides better mechanical integrity while not being cost prohibitive. In the frequency domain, in general, there are no particular advantages of overlap-dimple joint over the overlap joint. Specifically, for frequencies below 1.5 GHz, there is about 4 dB of less isolation than in the case of simple overlap-joint.

Traditionally, tongue and groove joint is relatively more complex than a butt joint having larger effective length. Effective length is defined as the tortuous path of the joint from outer surface to the inner surface as shown in Figure 1. Higher effective length produces better shielding when compared to the other joints. This added attraction makes it better candidate for selection of appropriate joint. The two-dimple joint having the smallest effective length provides the least shielding.

Looking at the same joint with 25% filled stainless steel fibers in the PC, a different pattern is observed (see Fig. 9). The overlap-dimple joint performs generally worse than simple overlap joint. On the other hand, the two-dimple joint performs best between frequencies of 1.2 to 2.4 GHz, among all the investigated joints presented in this figure. The trend, however, is reversed for frequencies above 2.8 GHz. Except for this change of direction, tongue and groove is the best choice for frequencies below 1.2 and 2.7–3.7 GHz.

In the case of electroless plated 20%-filled nickel-coated graphite polycarbonate, as presented in Figure 10, a general reduction of shielding effectiveness as the frequency of operation increases is observed. A substantial increase in the shielding property is noted in comparison to plain 20%-filled nickel-coated graphite. This is mainly due to higher conductivity of joined parts as well as high surface conductivity of the plated material.

The comparison of the two joints, namely, overlap and two-dimple joints reveals that at lower frequencies (up to 1.6 GHz) the overlap joint performs better than two-dimple joint. This trend also continues for frequencies between 2.2–3.3 GHz. However, in the rest of the frequency range, the two-dimple joint shows a better result.

In many applications such as simple mechanical assembly, cost effective joints similar to overlapping joint is desired and used. Figure 11 represents shielding effectiveness of four different materials used to make the joined part. Similar to

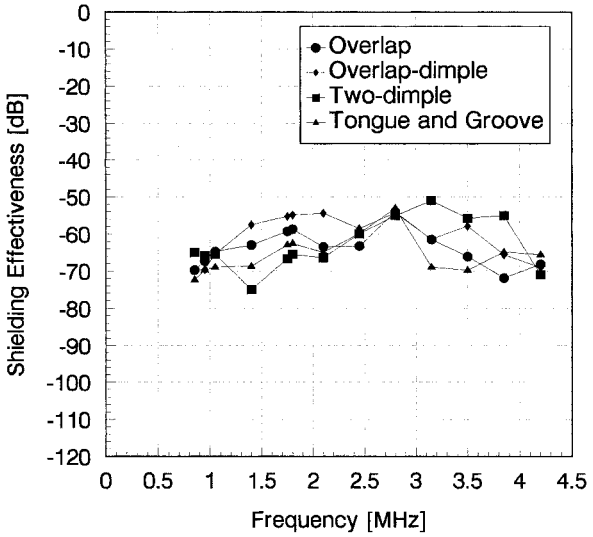

Figure 9 Shielding effectiveness of 25%-filled stainless steel in polycarbonate having various joint configurations.

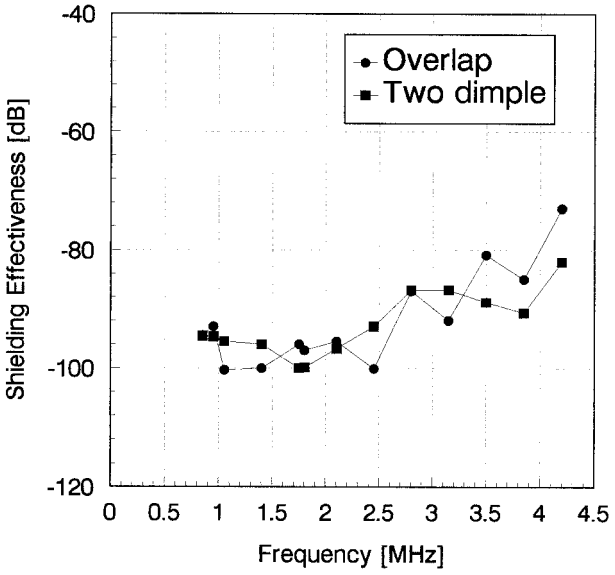

Figure 10 Shielding effectiveness of metalized 20%-filled nickel-coated graphite in polycarbonate having various joint configurations.

the other experiments, the nickel-coated graphite (ncg)-filled polymers perform better than stainless steel based polymers. Aluminum performs up to 30 dB better than the polymer based materials. The interesting item in this figure is the increased shielding effectiveness of the joint made of ncg-filled polycarbonate when it is metalized (electroless metalization) with copper and nickel. A gain of 30 dB in most frequencies below 4 GHz is observed. The fundamental reason for this major gain is in the absorption and reflection properties of this kind of materials. Paying attention to the following fundamental equation of reflection portion of the shielding effectiveness,

$$R_p = 168 - 10\ \mathrm{Log}(\mu_r f/\sigma_r)\ dB, \qquad (14)$$

one can deduct that the larger the μ_r, the smaller the reflection of the field from the polymeric materials. Similarly, the larger the σ_r, the larger the reflection of the plate. For a given frequency, reduction of the (μ_r/σ_r) ratio is desired. For aluminum, nickel, stainless steel, and copper, ratios of 1.64, 500, 25,000, and 1 are obtained, respectively. Thus, aluminum or copper produces the best results. Additionally, the absorption is calculated based on the following relation:

$$A = 8.69(t/\delta)\ dB \qquad (15)$$

where t is the thickness of the wall in inches, and δ is the skin depth in inches defined as

$$\delta = \frac{2.6}{\sqrt{f\mu_r\sigma_r}} \qquad (16)$$

The smaller the f, μ_r, or σ_r, the larger the absorption losses. For aluminum, nickel, stainless steel, and copper, the $\mu_r\sigma_r$ values are 0.61, 20, 10, and 1, respectively. For larger absorption, nickel or stainless steel should be used. Here, a combination of nickel and copper is selected mainly due to nonelectrical reasons. Additionally, since the material is plated, the rereflection is higher than the case of pure metals as can be deducted from the following equation:

$$B = 20\ \mathrm{Log}(1 - e^{-2t/\delta})\ dB. \qquad (17)$$

Monotonicity analysis of the above equation reveals that an increase in $\mu_r\sigma_r$ results in a decrease in the δ. Consequently, this decrease in the value increases the ratio of t/δ; thus reduces the rereflection loss.

From this analysis, it can be concluded that the choice of nickel and stainless steel is the best option. Here, because of dissimilarity between the above materials, the copper-nickel combination provides the best results when reflection, rereflection, and absorption are considered together. This analysis is simply driven for a case with no joint. In the current study, the effect of joint configuration plays a major role in reduction of shielding.

It should be noted that this mixed-metal-filled–

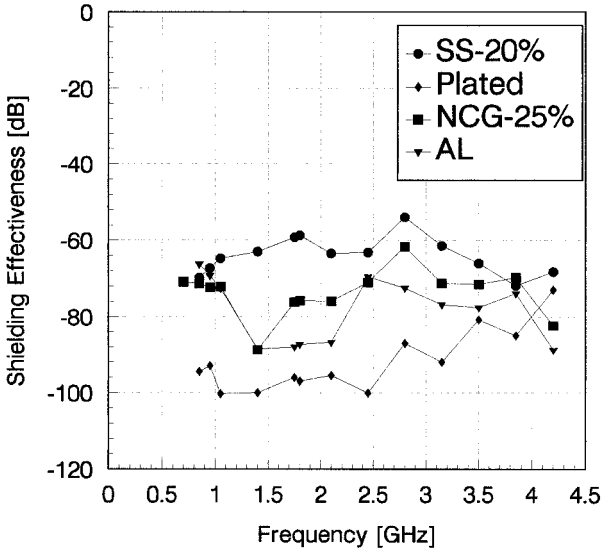

Figure 11 Shielding effectiveness of an overlap joint made of various materials.

Table I Coefficients of Eq. (18) for Calculation of Shielding Effectiveness

Joint Type	A	B	R
HPB (V)	59.275	−0.067	0.95
HRPVB (two dimple)	68.458	−0.036	0.96
HB (butt)	49.787	−0.122	0.94
HPVB (S)	71.224	−0.030	0.94
HRPB (one dimple)	51.706	−0.079	0.96

metalized technique is not readily attempted by other investigators, based on the authors' best knowledge.

Selecting aluminum as a metal of choice for the rest of the present work, the following results are obtained. Comparing five different joints made of aluminum, namely, the hermaphrodite raised peak butt (one-dimple), hermaphrodite peak valley butt (S), hermaphrodite peak butt (V), hermaphrodite raised peak valley butt (two-dimple), and butt joints, having a gap between the mating parts, the following equation is obtained.

$$\mathrm{SE} = A(S)^B \tag{18}$$

where S (in inches) is the gap generated between the two mating joints, and SE is the mean shielding effectiveness of the joint. The coefficients A and B are also tabulated and shown in Table I. The above correlation indicates a loss of shielding effectiveness when the gap between the mating parts are present. In this table, R represents the regression coefficient.

The results of various joints, namely, butt, slanted, S, one-dimple, and two-dimple joints, indicate that the shielding effectiveness is not only a function of effective length,[33] but also is a function of shape factor of the joint. A simplified equation relating the mean shielding effectiveness to the effective length and the joint shape factor is represented in the following equation:

$$\mathrm{SE} = 70.62*(\gamma)^{(0.14)} - 1023.0 + 3190.1(\mathrm{SF}) - 3674.9(\mathrm{SF})^2 + 1851.5(\mathrm{SF})^3 - 343.7(\mathrm{SF})^4 \tag{19}$$

where SF is the shape factor, and γ is the ratio of effective length of a particular joint to the reference joint ($L_{\mathrm{eff}}/L_{\mathrm{eff},r}$). These values are presented in Table II. The above-mentioned equation is correlated for metal-based joints. The results further reveal that the shielding effectiveness increases with increased effective length and shape factor. It is further assumed that the gap between the mating joints are maintained to be less than 0.025 mm. Shape factor is a subjective value assigned to each geometry varying from 1.0 to 2.0. The lower amount is selected for the butt joint, and the higher value is used for the solid material having no joint. Thus, the maximum value that a joint can have does not exceed 2.0 regardless of its complexity. The following equations describe the relationship to be used in calculation of shape factors:

For a noncurved joint, knowing the number of change in the joint surface direction (DIR), SF is defined as

$$\mathrm{SF} = 0.963 + 0.329(\mathrm{DIR}) - 0.0277(\mathrm{DIR})^2 \tag{20}$$

For the case of the S joint, the shape factor is 1.8. Here DIR is equal to three, since it has three-directional change in the joint configuration.

In the curved-member joint case (CM), the following equation is used:

$$\mathrm{SF} = 0.9748 + 0.437(\mathrm{CM}) - 0.04823(\mathrm{CM})^2 \tag{21}$$

The two-dimple joint has a shape factor of 1.7. Here CM is equal to two since there are two curved members in the joint. In the case of combination of both type of joints, the least value of shape factors, calculated from the above equations, is chosen by substituting the combined CM and DIR in each equation. For instance, in the

Table II The Shape Factors and Effective Lengths of Various Joints

Joint	SBJ (Butt) Joint	HSJ (Slanted) Joint	HPVBJ (S) Joint	HRPJ (One Dimple) Joint	HRPVBJ (Two Dimple) Joint
Effective length	1	1.15, 1.41, 2	2	1.4	1.344
Shape factor	1.0	1.2	1.8	1.3	1.7

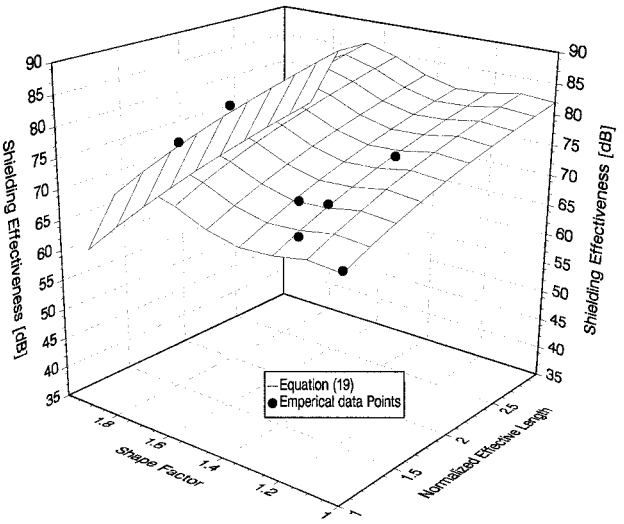

Figure 12 Influence of effective length and shape factor on the shielding effectiveness of joints.

determination of shape factor for a joint with a two-dimple and *S* configuration, a value of five (5) is inserted for both CM and DIR. Consequently, the shape factor is calculated to be 1.9, which is the lowest value between 1.9 and 1.95. The shape factors above 2.0 are invalid.

Figure 12 depicts the plot of SE verses SF and L_{eff}. In this figure, selected empirical data is also shown, which agrees well with the correlated equation.

CONCLUSIONS

Three enclosure material choices, namely, aluminum, filled, and plated polycarbonate, are examined to determine the best selection of joint materials in electronic equipment design for high shielding effectiveness. Increasing the geometric complexity of a joint, such as its effective length and shape factors, have a positive influence on shielding effectiveness. The tongue and groove joint provides the best shielding, while the raised-lap joint results in an adequate shielding with better mechanical strength without the use of screws. Correlations relating the effective length of a joint and shape factor to the shielding effectiveness are also presented. Introduction of metalization in addition to metal-filled polymers provides a very good shielding value, which decreases exponentially with increasing frequency. A reduction of shielding effectiveness caused by introduction of gap in the mating parts are observed. In addition, a strong dependency between the shielding effectiveness and the frequency of operation is evident.

This work has in part been supported by Bell Laboratories at Lucent Technologies and Design and Manufacturing Institute at Stevens Institute of Technology. Their support are greatly appreciated.

REFERENCES

1. B. D. Mottahed and S. Manoochehri, *Polym. Plastic Tech. Eng.,* **34,** 271–346 (1995).
2. Li Lin and D. D. L. Chung, 5th Inter. SAMPE Electronics Conf., Vol. 5, Society for the Advancement of Material and Process Engineering.
3. Y. Trenkler and L. E. McBride, 1990 Int. Symp. on Electromagnetic Compatibility, Symposium Record, p. 1–4.
4. B. Chuba, *Plating Surf. Finishing,* **76,** 30–33 (1989).
5. D. D. L. Chung and Q. J. Zheng, *Comp. Sci. Tech.,* **36,** 1–6 (1989).
6. S. R. Gary, *Midcon / 81 Conference Record,* Chicago, IL, Nov. 10–12, 1981.
7. F. Matsui, T. Okada, T. Kawakubo, and T. Otaka, Proc. 77th AESF Ann. Tech. Conf., Part 2.
8. S. Naik, M. Carmel, and M. Fenton, Tech. Sessions of the 41st Ann. Conf.–Reinforced Plastics/Composites Institute, Reinforced Plastics/Composites Institute, 1986.
9. J. P. Kosiarski, 1984 Int. Symp. on Electromagnetic Compatibility, Vol. 1, pp. 524–7.
10. S. M. Museameh, M. K. Abdelazeez, M. S. Ahmad, A. M. Zihlif, M. Malinconico, E. Martuscelli, and G. Ragosta, *Mat. Sci. Eng. B, Solid-State Mat. Adv. Tech.,* **B10,** pp. 29–33 (1991).
11. D. K. Chen, Chin-Chi Ma, and A. T. Hu, 36th Int. SAMPE Symp. and Exhibition, Vol. X Society for the Advancement of Material and Process Engineering, pp. XXX–XXX.
12. A. L. Holbrook, 1985 Ann. Powder Metallurgy Conf. Proc., pp. 679–684.
13. F. Pagano, *Elec. Packaging and Prod.,* **22,** 268–74 (1982).
14. Y. Seki and S. Nitta, *Int. Symp. Electromagnetic Compatibility, EMC 89,* pp. 306–311, 1989.
15. S. B. Railkar, H. S. Gokturk, and D. M. Kalyon, *J. Reinf. Plastics Comp.,* **12,** 1212–1220 (1993).
16. R. P. Jedlicka, S. P. Castillo, and L. K. Warne, *Antennas and Propagation Soc. Symp.,* pp. 889–892, June 1991.
17. D. S. Gedney and R. Mittra, *IEEE Trans. Electromag. Compatibility,* **34,** 404–415 (1992).
18. A. T. Auckland and R. F. Harrington, *IEEE Trans. Microwave Theory Tech.,* **MTT-28,** 548–555 (1980).

19. E. Honig, *IEEE Trans. Electromag. Compatibility,* **EMC-19,** (1977).
20. R. Mohr, *IEEE Symp. EMC,* 1987.
21. D. Merewether, *IEEE Symp. EMC,* 1985.
22. S. Miyake, Y. Umezu, Y. Sagawa, T. Moritia, and R. Yoshino, *IEEE Int. Symp. EMC,* pp. 120–125, 1991.
23. T. Senior and Volakis, *IEEE Trans. Antennas Propogat.,* **37,** 744–750 (1989).
24. T. Senior, K. Sarabandi, and J. Natzke, *IEEE Trans. Antennas Propogat.,* **38,** 1102–1110 (1990).
25. S. Jeng and S. Tzeng, *IEEE Trans. Antennas Propogat.,* **39,** 661–664 (1991).
26. M. Murthy, *ANTEC'87,* pp. 300–304, 1987.
27. G. Pettit, *Westcon Conference Record,* pp. 348–351, 1989.
28. R. Steinfeld, *Proc. EMC '86,*
29. *D. Auckland and R. Harrington, IEEE Trans. Microwave Theory Tech.,* **MTT-26,** 499–505 (1978).
30. L. Warne and K. Chen, *IEEE Trans. EMC,* **32,** 217–221 (1990).
31. J. E. Bridges, *IEEE Trans. EMC,* **30,** 211–221 (1988).
32. C. Vitek, *IEEE 1989 Nat. Symp. on EMC,* 1989.
33. B. D. Mottahed and S. Manoochehri, *IEEE Tran. Components and manu. Tech. B, Adv. Packaging,* **19,** 238–248 (1996).
34. P. Wilson and M. T. Ma, *EMI, RFI Shielding Plastics, R. Tech. Conf.,* pp. 9–18, 1984.
35. L. O. Hoeft and J. S. Hofstra, *IEEE Int. Symp. EMC,* pp. 158–160, 1986.
36. L. O. Hoeft and J. S. Hofstra, *IEEE Trans. EMC,* 326–340 (1988).
37. K. Lee, *EMP Interaction: Principles, Techniques, and Reference Data,* Hemisphere Publishing Corp., 1986.